

## Invited Research Article

# Hydrothermal pressure-temperature control on CO<sub>2</sub> emissions and seismicity at Campi Flegrei (Italy)

G. Chiodini<sup>a,\*</sup>, S. Caliro<sup>b</sup>, R. Avino<sup>b</sup>, G. Bini<sup>c</sup>, F. Giudicepietro<sup>b</sup>, W. De Cesare<sup>b</sup>, P. Ricciolino<sup>b</sup>, A. Aiuppa<sup>d</sup>, C. Cardellini<sup>e,a</sup>, Z. Petrillo<sup>b</sup>, J. Selva<sup>a</sup>, A. Siniscalchi<sup>f</sup>, S. Tripaldi<sup>f</sup>

<sup>a</sup> Istituto Nazionale di Geofisica e Vulcanologia, Sezione di Bologna, via D. Creti 12, 40128 Bologna, Italy

<sup>b</sup> Istituto Nazionale di Geofisica e Vulcanologia, Sezione di Napoli Osservatorio Vesuviano, via Diocleziano 328, 80124 Napoli, Italy

<sup>c</sup> Institute of Geochemistry and Petrology, ETH Zürich, Clausiusstrasse 25, 8092 Zürich, Switzerland

<sup>d</sup> Dipartimento di Scienze della Terra e del Mare (DiStEM), Università degli Studi di Palermo, via Archirafi 22, 90123 Palermo, Italy

<sup>e</sup> Dipartimento di Fisica e Geologia, Università degli Studi di Perugia, via Pascoli snc, 06123 Perugia, Italy.

<sup>f</sup> Dipartimento di Scienze della Terra e Geoambientali, Università degli Studi di Bari, Aldo Moro, via Edoardo Orabona, 4, 70125 Bari, Italy

## ARTICLE INFO

## Article history:

Received 16 December 2020

Received in revised form 19 March 2021

Accepted 27 March 2021

Available online 30 March 2021

## Keywords:

Volcanic unrest

Hydrothermal systems

Campi Flegrei

Fumarole compositions

CO<sub>2</sub> emission

Volcano seismicity

## ABSTRACT

Fluids supplied by stored magma at depth are causal factors of volcanic unrest, as they can cause pressurization/heating of hydrothermal systems. However, evidence for links between hydrothermal pressurization, CO<sub>2</sub> emission and volcano seismicity have remained elusive. Here, we use recent (2010–2020) observations at Campi Flegrei caldera (CFC) to show hydrothermal pressure, gas emission and seismicity at CFC share common source areas and well-matching temporal evolutions. We interpret the recent escalation in seismicity and surface gas emissions as caused by pressure-temperature increase at the top of a vertically elongated (0.3–2 km deep) gas front. Using mass (steam) balance considerations, we show hydrothermal pressurization is causing energy transfer from the fluids to the host rocks, ultimately triggering low magnitude earthquakes within a seismogenic volume containing the hydrothermal system. This mechanism is probably common to other worldwide calderas in similar hydrothermal activity state.

© 2021 Published by Elsevier B.V.

## 1. Introduction

The injection, ascent, storage and surface release of deep fluids in the upper crust are widespread phenomena in nature, and are recurrent drivers of geological catastrophes. Fluid pressure increase in the upper crust can trigger seismicity reducing the effective normal stress on fault planes (e.g., Hubbert and Rubey, 1959; Sibson, 1992; Miller, 2013), and the recurrently observed co-seismic variations in gas flux and composition (Fischer et al., 2017; Girault et al., 2018; Chiodini et al., 2020) are clear hints for a cause-effect link between fluids and earthquakes. It is also well-established that artificial fluid injection in the subsurface, and the consequent fluid pressure increase, can lead to seismicity (Ellsworth, 2013; Keranen and Weingarten, 2018).

Volcanoes make no exception, the most notable example being that of Mammoth Mt. (California), when the sudden surface burst (in 1990) of huge amounts of volcanic-hydrothermal CO<sub>2</sub> associated to a seismic crisis killed a large portion of the forest (Farrar et al., 1995; Sorey et al., 1998), and repeated increases in diffuse CO<sub>2</sub> emissions

accompanied seismic swarms in the subsequent years (Lewicki et al., 2014; Werner et al., 2014; Hotovec-Ellis et al., 2018; Pfeiffer et al., 2018).

Volcanoes are especially suitable natural laboratories for investigating fluid flow - pressure - earthquake associations, because robust and relatively continuous geochemical and geophysical datasets are available. One aspect that is especially relevant to restless volcanoes is that injected fluids are generally hot and H<sub>2</sub>O-rich so that, upon ascent, can interact with, and condense into, hydrothermal aquifers: the heating and consequent volumetric expansion of the hosting rocks that result from condensation of such magmatic steam is a potential additional seismicity driver during volcanic unrest (Chiodini et al., 2015).

The relations among hydrothermal temperature-pressure, fluid flow and earthquakes are here investigated at Campi Flegrei (CFC, Fig. 1a), a restless resurgent caldera formed ~39 kyrs ago by the largest caldera-forming eruption in Europe in the last 200 kyrs (Costa et al., 2012). CFC exhibits (since the 1950s) repeated inflation periods (Orsi et al., 1999; Del Gaudio et al., 2010) and seismic crises, which have worried the scientific community as much to suggest an eruption is approaching (Selva et al., 2012; Kilburn et al., 2017). The CFC is undergoing since 2004 a new inflation phase (total maximum vertical displacement of ~0.75 m by the time of writing), associated with frequent shallow seismicity, part of which interpreted as originating from fluid transfer

\* Corresponding author.

E-mail address: [giovanni.chiodini@ingv.it](mailto:giovanni.chiodini@ingv.it) (G. Chiodini).

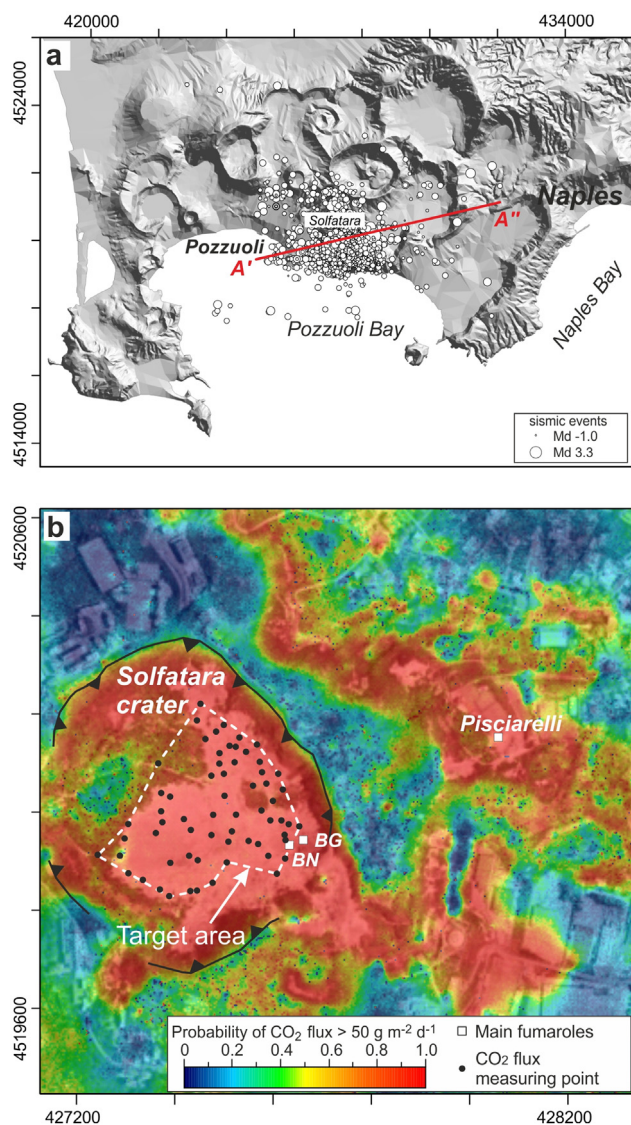


**Fig. 1.** Location map. a) Campi Flegrei caldera and location of the 2004–2020 earthquakes. The A'-A'' line refers to the vertical section reported in Fig. 6. b) Map of the Solfatara diffuse degassing structure (DDS) showing the locations of the target area, the monitored 63 points and the main fumaroles. The map, based on 13,158 CO<sub>2</sub> flux measurements from 1998 to 2016 (Cardellini et al., 2017), illustrates the probability that the simulated CO<sub>2</sub> flux is greater than 50 g m<sup>-2</sup> d<sup>-1</sup>, selected as the threshold for a pure biogenic CO<sub>2</sub> flux. Coordinates are expressed in UTM-WGS84.

processes (Bianco et al., 2004; Saccorotti et al., 2007; D'Auria et al., 2011; Chiodini et al., 2017a; Giudicepietro et al., 2020). At the same time, large compositional variations are being observed in the fumarolic effluents (Caliro et al., 2014; Chiodini et al., 2016), and marked flux increases are being registered in hydrothermal CO<sub>2</sub> release from both fumarolic vents (Tamburello et al., 2019) and soil diffuse degassing structures (Cardellini et al., 2017). The escalating CO<sub>2</sub> emissions, and the concomitant compositional changes in the fumaroles, have been interpreted as signs that magma degassing at depth may have reached a critical condition in which heating and pressurization of the shallower Cfc hydrothermal system is occurring at accelerating rate (Caliro et al., 2014; Chiodini et al., 2015, 2016). In 2012, the evolution of the monitored geophysical and geochemical parameters induced the Italian Civil Protection (DPC) to raise the Cfc alert level from green (calm) to yellow (attention).

Here, we characterise the recent pressure-temperature (P-T from here on) evolution in the Cfc hydrothermal system, as inferred from geochemical modelling of fumarolic compositions, and to explore its

temporal link with the rates of deeply derived CO<sub>2</sub> emissions and seismicity. To this aim, our multidisciplinary analysis combines results for the chemical compositions of the Cfc fumaroles with a set of variables related to the gas emission, and the earthquakes. We exclude from our analysis the deformation signals, as their main source area is thought to be deeper than the hydrothermal system this work is focussed on (3–4 km; Amoroso et al., 2014a, 2014b).

Geochemical data (fumarolic compositions and CO<sub>2</sub> fluxes) refer to the hydrothermal sites of Solfatara and Pisciarelli (Fig. 1). Solfatara, a tuff cone formed about 4 ka ago (Smith et al., 2011), is the most active degassing zone of the Cfc, being site of numerous fumarolic vents and of a widespread soil diffuse degassing of hydrothermal-volcanic CO<sub>2</sub> (Chiodini et al., 2001; Cardellini et al., 2017; Fig. 1b). The most recent CO<sub>2</sub> flux measurements performed over the entire zone identify a ~ 1 km<sup>2</sup> wide area diffusively emitting deeply derived CO<sub>2</sub> (the so called Solfatara Diffuse Degassing Structure, Solfatara DDS, Chiodini et al., 2001; Fig. 1b). The typical CO<sub>2</sub> flux sustained by the DDS was 1000–2000 t d<sup>-1</sup> in 2014–2016 period (Cardellini et al., 2017). Significant amounts of CO<sub>2</sub> are also emitted by fumarolic vents, the most active of which are located in the eastern slope of the Solfatara cone (Pisciarelli vents, CO<sub>2</sub> emission up to 600 t d<sup>-1</sup> in 2019 (Tamburello et al., 2019) and inside the Solfatara depression (BG and BN vents, CO<sub>2</sub> emission up to ~300 t d<sup>-1</sup> in 2013; Aiuppa et al., 2013; Pedone et al., 2014; Fig. 1b).

After a description of the evolution over time of different parameters we attempt an integrated analysis aimed at understanding the impact of hydrothermal fluid P-T changes on earthquakes occurrence and fluid emissions.

## 2. Databases

The databases used in this work (Supplementary Data File S1) are here briefly described.

### 2.1. Chemical compositions of Solfatara fumaroles

The main and hottest fumaroles of Solfatara, BG ( $T = 150\text{--}165\text{ }^{\circ}\text{C}$ ) and BN ( $T 140\text{--}150\text{ }^{\circ}\text{C}$ ) (Fig. 1b), have been systematically sampled since 1983 and 1995, respectively. The dataset includes the temperature and chemical compositions (H<sub>2</sub>O, CO<sub>2</sub>, H<sub>2</sub>S, Ar, N<sub>2</sub>, H<sub>2</sub>, CH<sub>4</sub> and CO) of gas samples taken and analysed with similar procedures, from 1983 to 2020 (see Caliro et al., 2007; Cioni and Corazza, 1981 for the sampling and analytical methods). This Solfatara fumarolic fluid database is unique for the large number of samples (671), for its continuity (~ 35 years of observations) and for the homogeneity of the sampling and analytical methods used. Different laboratories contributed to this database: the laboratories of CNR of Pisa that started the work at the beginning of 1980's; the laboratory of University of Perugia that analysed the gas samples in the middle 1990's; and the fluid geochemistry laboratory of Osservatorio Vesuviano from 1998 to 2020.

### 2.2. Diffuse CO<sub>2</sub> flux from the Solfatara crater target area

During April 2004–October 2020, 149 soil CO<sub>2</sub> flux campaigns have been performed inside the Solfatara crater. In total, the dataset consists of 9315 measurements performed with the accumulation chamber method (Chiodini et al., 1998) over a grid of 63 points whose location remained unchanged during the period (Fig. 1b). The data are reported in monthly surveillance reports of Osservatorio Vesuviano for the Civil Defence of Italy (<http://www.ov.ingv.it/ov/it/bollettini/275.html>). The results of the first 50 campaigns have already been published (Granieri et al., 2009), while the remaining are here reported for the first time. For each campaign, we computed the total CO<sub>2</sub> output (FCO<sub>2</sub> in t d<sup>-1</sup>) from the target area (Fig. 1b). The FCO<sub>2</sub> and its uncertainty were computed by applying a geostatistical method based on sequential Gaussian simulation (sGs; Cardellini et al., 2003) to the soil CO<sub>2</sub>

fluxes of the 149 campaigns. Specifically, we used the *sgsim* algorithm (GSLIB software library; Deutsch and Journel, 1998). The CO<sub>2</sub> flux has been simulated on a of 4 m x 4 m grid starting from variogram models fitting the experimental variograms of the normal scores of the CO<sub>2</sub> flux (for further details see Cardellini et al., 2003). For each campaign, 200 simulations were realised and the total CO<sub>2</sub> release was computed by summing the products of the simulated CO<sub>2</sub> flux value at each grid cell by the cell surface. The mean total CO<sub>2</sub> flux and its standard deviation, computed from the 200 realizations, are taken as FCO<sub>2</sub> and its uncertainty for each campaign. As an example, Supplementary Fig. 1 illustrates the CO<sub>2</sub> flux map obtained considering at each location the mean of the CO<sub>2</sub> fluxes measured in the 149 campaigns. The target area to which each FCO<sub>2</sub> estimate refers to (coloured area in Supplementary Fig. S1) was limited to the area within the outermost measuring points, in order to avoid uncertainties related to extrapolations to un-sampled zones.

### 2.3. Diffuse CO<sub>2</sub> flux from the Solfatara DDS

This dataset includes the total CO<sub>2</sub> output by diffuse degassing at Solfatara (FCO<sub>2</sub>-DDS) from 1998 to 2016 estimated from soil CO<sub>2</sub> flux measurements covering an area of 1.4 km<sup>2</sup> which includes Solfatara crater and Pisciarelli areas (Fig. 1b; Cardellini et al., 2017). The soil CO<sub>2</sub> fluxes were measured in 30 surveys using the accumulation chamber method (Chiodini et al., 1998) and the total CO<sub>2</sub> output was estimated applying a geostatistical method based on sGs (for further details see Cardellini et al., 2017).

### 2.4. CO<sub>2</sub> fluxes from Pisciarelli vents

This dataset is composed of twenty-one measurements of the CO<sub>2</sub> flux from the Pisciarelli vents performed by different authors during 2012–2019 (Aiuppa et al., 2013; Pedone et al., 2014; Aiuppa et al., 2015; Quei ser et al., 2017; Tamburello et al., 2019). Measurement methods are different and include: tunable diode laser absorption spectroscopy (Pedone et al., 2014), differential absorption lidar (Aiuppa et al., 2015), laser remote-sensing spectrometry (LARSS; Quei ser et al., 2017), multi-component gas analyzer system (MultiGAS; Aiuppa et al., 2013; Tamburello et al., 2019). The reader is referred to the original articles for the details on these different techniques. Tamburello et al. (2019) report an overall consistency of the CO<sub>2</sub> fluxes obtained with the different measurement methods.

### 2.5. Fumarolic tremor at Pisciarelli

The fumarolic tremor is a continuous seismic signal recorded in the vicinity of the Pisciarelli fumaroles, currently the largest of the Cfc. To record this signal, a seismic station was installed in 2010 about 8 m away from the main fumarolic vent. The fumarolic tremor, analysed in previous studies (Chiodini et al., 2017b; Giudicepietro et al., 2019, 2020), is polarized in the vertical direction and characterized by a spectral peak at around 10 Hz. To represent the temporal evolution of the tremor amplitude, the Real-time Seismic-Amplitude Measurement (RSAM; Endo and Murray, 1991) was calculated on 30-min windows of the vertical component signal, filtered in 5–15 Hz frequency band.

### 2.6. Air CO<sub>2</sub> concentrations at Pisciarelli

Since April 2007, an automatic station measures soil temperature, soil CO<sub>2</sub> fluxes, and CO<sub>2</sub> concentrations in air, at 40 cm height, 20 m downwind of the main Pisciarelli vent (Chiodini et al., 2017b). The April 2007–October 2020 daily air CO<sub>2</sub> concentrations are systematically higher than in ambient air (1000–5000 ppm vs ~ 400 ppm) due to persistent fumigation from the fumarolic plume.

### 2.7. Earthquakes

We used the Cfc earthquake locations available in the public-access INGV- Osservatorio Vesuviano database (<http://sismolab.ov.ingv.it/sismo/index.php?PAGE=SISMO/last&area=Flegrei>). Hypocentre locations were obtained using a 1D layered velocity model. The dataset consists of 2026 located earthquakes with magnitude (Md) ranging between -1.1 and 3.3, representing about 47% of the total number of Cfc earthquakes recorded by the INGV-Osservatorio Vesuviano permanent seismic network between January 2004 and October 2020. Seismicity is mostly concentrated in the Solfatara-Pisciarelli area (Fig. 1a) at relatively shallow depth and the magnitude of the events is generally low with only 16 events with 2.0 ≤ Md ≤ 3.3. From 2005 to 2012, earthquakes occurred mainly in swarms. Since 2012–2013, their occurrence rate has increased over time, both as swarms and as single events, with single events becoming more frequent in the last 2 years.

## 3. Results and discussion

### 3.1. Pressure-temperature geoindicators based on fumarole compositions

Solfatara fumaroles emit vapours characterized by the absence of acidic gas species (i.e., SO<sub>2</sub>, HCl, HF) that are typical of high-temperature magmatic gas emissions. They also exhibit detectable amounts of species formed in the hydrothermal environment (e.g., CH<sub>4</sub>). These compositions suggest fumarolic steam originates from a hydrothermal system in which the original magmatic acidic components have already been removed by scrubbing processes (Cioni et al., 1984; Caliro et al., 2007). Since 1984, the Solfatara compositional database was used to derive the T-P conditions of this hydrothermal system (e.g., Cioni et al., 1984; Chiodini et al., 1996, 2015, 2016; Caliro et al., 2007). Recently, two different geochemical approaches have lead to contrasting results and different implications for the current Cfc unrest, which has been interpreted as either driven by pressurization of the Cfc system (Chiodini et al., 2015, 2017a), or associated with a general depressurization of the hydrothermal system (Moretti et al., 2017) (Fig. 2). We refer to the two approaches, which stand on different model assumptions, as the *no-condensation* (Moretti et al., 2017) and *vapour-liquid coexistence* (Chiodini et al., 2015) models.

#### 3.1.1. The no-condensation model

Moretti et al. (2017) applied a model originally developed by Chiodini et al. (1996) and then refined by Chiodini and Marini (1998). The geobarometric and geothermometric relations are derived considering the formation reactions of H<sub>2</sub>, CO and CH<sub>4</sub> from the main species H<sub>2</sub>O and CO<sub>2</sub>:



whose equilibrium constants are expressible as:

$$\log K_{\text{H}_2} = \log f_{\text{H}_2} + 1/2 \log f_{\text{O}_2} - \log f_{\text{H}_2\text{O}} \quad (4)$$

$$\log K_{\text{CO}} = \log f_{\text{CO}} + 1/2 \log f_{\text{O}_2} - \log f_{\text{CO}_2} \quad (5)$$

$$\log K_{\text{CH}_4} = \log f_{\text{CH}_4} + 2 \log f_{\text{O}_2} - \log f_{\text{CO}_2} - 2 \log f_{\text{H}_2\text{O}} \quad (6)$$

where  $\log K_{\text{H}_2} = -12,707/T + 2.548$ ,  $\log K_{\text{CO}} = -14,955/T + 5.033$  and  $\log K_{\text{CH}_4} = -42,007/T + 0.527$  (thermodynamic data from Stull et al., 1969; T in Kelvin). Suitable combinations of eqs. 4, 5 and 6 allow to eliminate the log  $f_{\text{O}_2}$  variable and to derive the following geothermometric and geobarometric functions:



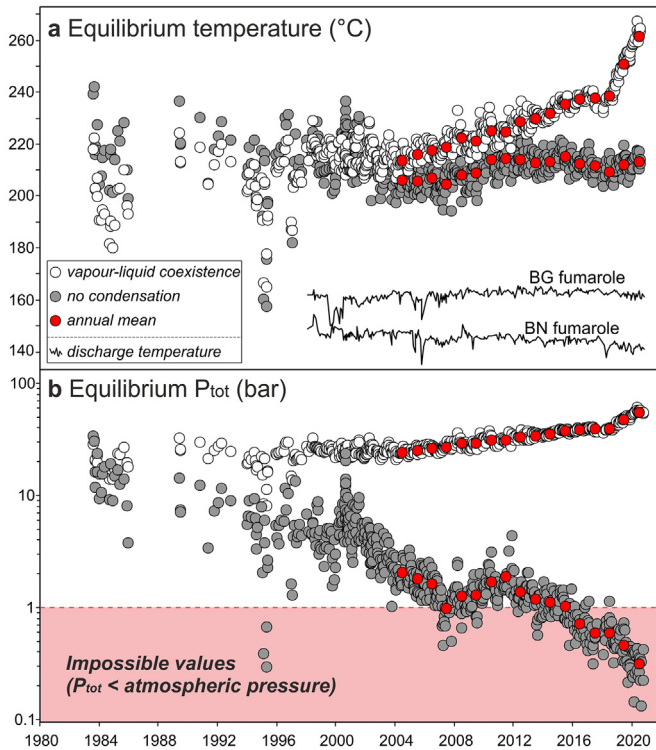


**Fig. 2.** T-P estimates. a) Equilibrium temperatures and b) pressures estimated with two alternative geochemical models (see the text) from the 1983–2020 compositions of BG and BN fumaroles. The discharge temperatures of the fumaroles are reported in panel a.

$$T = -2248 / (\log (X_{CO} / X_{CO_2}) + \log (X_{H_2O} / X_{H_2}) - 2.485) \quad (7)$$

$$\log P_{H_2O} = (19.605 - \log (X_{CO}^4 / (X_{CH_4} \times X_{CO_2}^3)) - 17813/T) / 2 \quad (8)$$

where the equimolar ratios of the measured fumarolic molar fractions ( $X_i$ ) are assumed equal to the fugacities ratios and  $P_{H_2O} \sim f_{H_2O}$ .

Finally considering the Dalton law,

$$P_{CO_2} = P_{H_2O} X_{CO_2} / X_{H_2O} \quad (9)$$

$$P_{tot} \sim P_{CO_2} + P_{H_2O} \quad (10)$$

Relevant assumptions of this approach are: (i) the redox conditions are internally fixed within the  $H_2O$ - $CO_2$ - $H_2$ - $CO$ - $CH_4$  gas system, an assumption that implies that  $CH_4$  equilibrates at the same T-P conditions as the kinetically faster species  $H_2$  and  $CO$  (Giggenbach, 1987); (ii) no secondary processes affect  $H_2O$  (condensation and/or water addition). Because the contrasting results with the model of Chiodini et al. (2015) strongly depends on this last assumption, we name the model used by Moretti et al. (2017) as the *no-condensation* model.

### 3.1.2. The vapour-liquid coexistence model

Caliro et al. (2007), showed in a  $\log H_2/H_2O$  vs  $\log CO/CO_2$  stability diagram (Fig. 5 in Caliro et al., 2007) that Solfatara fumaroles plot close to a typical hydrothermal redox buffer (DP; D'Amore and Panichi, 1980) at temperature of 200–250 °C and far from the  $H_2S$ - $SO_2$  redox buffer of volcanic gases (Giggenbach, 1987). The same authors, considering the carbon isotopic exchange reaction between  $CO_2$  and  $CH_4$ , demonstrated that the  $CH_4/CO_2$  ratio reflects temperatures (360–430 °C) much higher than those returned by the  $H_2/H_2O$  and  $CO/CO_2$  ratios, a fact that in principle excludes the possibility of using  $CH_4$ ,  $CO$  and  $H_2$  in a unique geothermometric function. Furthermore, starting from early 2000's, macroscopic evidences suggested the

occurrence of secondary processes (i.e., steam condensation) affecting the fumarolic  $H_2O$  content: (i) the almost continuous increase in the non-condensable gas fraction relative to water (Chiodini et al., 2015); (ii) a systematic increase of the  $CO/CO_2$  ratio (an indicator of hydrothermal temperature, and condensation is very efficient to heat a hydrothermal system); (iii) the pervasive circulation of condensates underneath Solfatara crater, and in particular close to the main fumaroles BG and BN (Bruno et al., 2007; Byrdina et al., 2014; Gresse et al., 2017); (iv) the formation of strong boiling pool of condensates and repeated episodes of liquid/mud emission at Pisciarelli (Chiodini et al., 2015).

In order to avoid the effects of these secondary processes affecting  $H_2O$ , and in order to exclude  $CH_4$  from the model, Chiodini et al. (2015) derived T-P functions from eqs. 4 and 5 based on equimolar ratios between non-condensable gases ( $H_2$ ,  $CO$ ,  $CO_2$ ). The derivation of the geothermometric and geobarometric function was possible considering (i)  $f_{H_2O}$  fixed by the vapour-liquid coexistence and (ii)  $f_{O_2}$  as a function of the temperature. Redox conditions of Solfatara gases were assumed to be controlled by the DP buffer ( $\log f_{O_2} = 8.20 - 23,643/T$ ). According to Chiodini and Marini (1998), an alternative  $f_{O_2}$ -T function applicable to Solfatara fumarolic gases is the 'Campanian Volcanoes' buffer (CV,  $\log f_{O_2} = 7.75 - 23,169/T$ ). The correspondent geothermometric relations are:

$$T = 3133.5 / (0.933 - \log X_{CO} / X_{CO_2}) \quad (11)$$

valid for redox conditions controlled by the DP relation, and

$$T = 3370.5 / (1.158 - \log X_{CO} / X_{CO_2}) \quad (12)$$

when considering the CV redox buffer.

The geobarometric functions are:

$$\log P_{H_2O} = 5.510 - 2048/T \quad (13)$$

where the water pressure is assumed equal to water fugacity of saturated vapour (i.e., vapour-liquid coexistence for pure water (Giggenbach, 1980)),

$$\log P_{CO_2} = 3.025 + 201/T - \log X_{H_2} / X_{CO} \quad (14)$$

derived by a linear combination of eqs. 4 and 5, and,

$$P_{tot} \sim P_{CO_2} + P_{H_2O} \quad (15)$$

Use of either the DP or the CV  $f_{O_2}$ -T relation results into different P-T estimations. In agreement with Chiodini et al. (2015), we use the DP option (eq. 11) that, for the post 2010 period considered in this work, outputs T values from 218 °C to 267 °C and P from 27 to 60 bar; while the alternative eq. 12 (CV buffer) returns higher T and P values (238 °C - 287 °C, 37 bar - 78 bar). We stress, however, that these systematic differences do not affect the results and considerations of our work that is based on the relative variation of the normalized T-P values that are practically the same for both the DP and CV estimations.

We will refer to this model as the *vapour-liquid coexistence* model.

### 3.1.3. Temperature-pressure estimations

The T-P estimates, derived by the two models for the entire Solfatara fumaroles' database, are contrasted in the chronograms of Fig. 2.

Even though, any model can not be considered completely reliable because it is necessarily based on some a-priori assumptions, the *no-condensation* model is certainly not reliable because the total estimated pressures ( $P_{tot} = P_{H_2O} + P_{CO_2}$ ) for the post-2015 samples are impossible as systematically below atmospheric pressure (<1 bar, Fig. 2b).

The reliability of the *vapour-liquid coexistence* model is tested below by comparing the inferred P-T conditions with different independent fluid flow related variables, and with the earthquake occurrence at CFC.

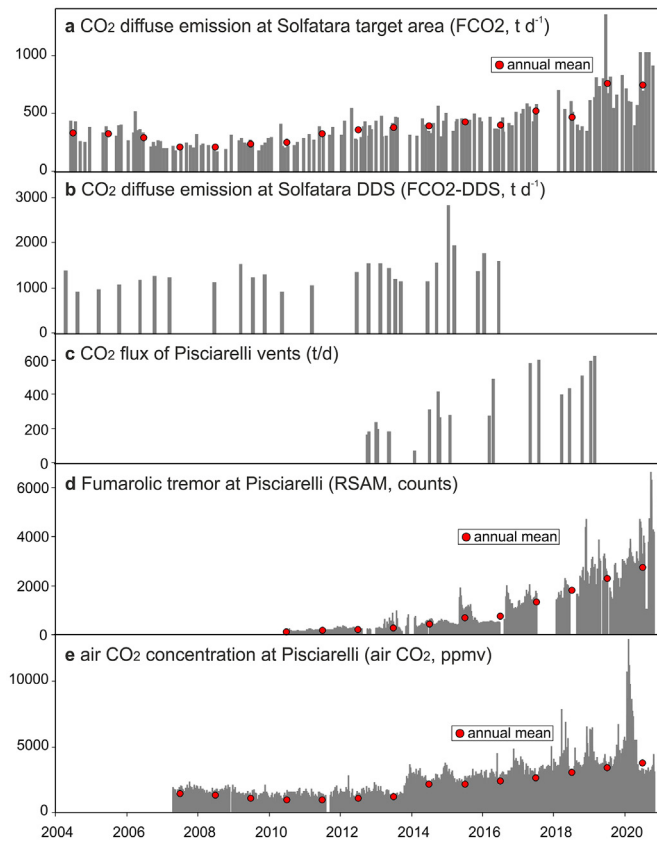


Fig. 3. Chronograms of the FFR variables. Annual means are reported with red symbols.

### 3.2. Fluid flow related (FFR) variables

Figs. 3a, b, c, d and e are chronograms of the available FFR variables that we take as proxies for the CO<sub>2</sub> degassing regime of the Solfatara-Pisciarelli area. In particular the CO<sub>2</sub> flux (FCO<sub>2</sub>, Fig. 3a) from the Solfatara target area (see Fig. 1b) and the total CO<sub>2</sub> flux from the entire Solfatara DDS (FCO<sub>2</sub>-DDS, Fig. 3b; Cardellini et al., 2017) are representative of the diffuse emission. Numerous FCO<sub>2</sub> data (149) are available for the entire observation period (2004–2020) while

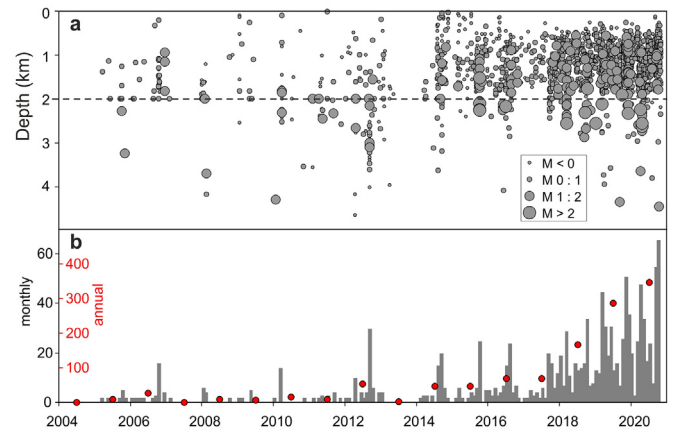


Fig. 5. CFC earthquakes from 2004 to October 2020. a) Chronogram of depths and magnitudes. b) Monthly (gray histogram) and annual (red symbols) number of earthquakes with Magnitude > 0.1; the 2020 annual number of earthquakes has been scaled over the entire year.

FCO<sub>2</sub>-DDS measurements are less frequent (Cardellini et al., 2017) and not available since 2017.

The CO<sub>2</sub> flux from Pisciarelli vents (Fig. 3c; Tamburello et al., 2019), the fumarolic tremor at Pisciarelli (RSAM, Fig. 3d) and the CO<sub>2</sub> concentrations in air at Pisciarelli (air CO<sub>2</sub>, Fig. 3e) are taken as proxies of the vent emission in the area. Although not direct flux measurements, RSAM and air CO<sub>2</sub> are almost continuously acquired, and their temporal fluctuations have previously been shown to scale with the intensity of hydrothermal activity at Pisciarelli (Fig. 4; Chiodini et al., 2017b; Giudicepietro et al., 2019, 2020).

### 3.3. 2004–2020 earthquakes occurrence at CFC

We refer here to the earthquakes occurred at CFC from 2004 to October 2020 (Fig. 1a) whose locations and magnitudes are available in public databases of the Osservatorio Vesuviano (<http://www.ov.ingv.it/ov/it/banche-dati.html>). It is worth to note that the events concentrate underneath the Solfatara-Pisciarelli (Fig. 1a) and are in general of low magnitude (maximum magnitude = 3.3) and of relatively shallow depths (Fig. 5a). The earthquakes' occurrence rate manifestly increases since 2017–2018 (Fig. 5b). Note that Fig. 5b

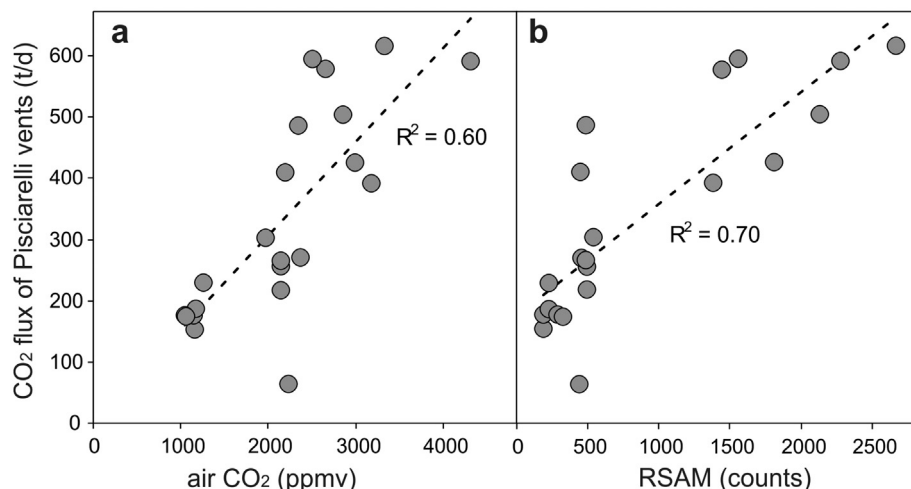


Fig. 4. Air CO<sub>2</sub> and RSAM vs CO<sub>2</sub> flux of Pisciarelli vents. RSAM and air CO<sub>2</sub> are reported as the mean values measured at the time of the CO<sub>2</sub> flux campaign  $\pm$  30 days.

reports events with magnitude  $\geq 0.1$ , for which the catalogue is reasonably complete in the observation period. The absence of deep events at Cfc (i.e., depth  $> 3\text{--}4$  km) likely reflects the high temperatures expected at depth, and a very shallow brittle-ductile transition ( $3\text{--}5$  km; Castaldo et al., 2019).

### 3.4. Comparison of the different datasets

A multivariate time-series analysis is attempted to compare the different observations. To this aim, we compute the annual mean (annual number for the earthquakes) of each variable (red points in Figs. 2, 3 and 5), focussing on the 2010–2020 period, for which most of the variables are available. The approach based on the analysis of the annual values has the advantage of filtering out any seasonally controlled variations. The multivariate analysis is not applied to the FCO2-DDS (Fig. 3b) and to the CO<sub>2</sub> flux from Pisciarelli vents (Fig. 3c) because these measurements are sporadic and not available for the entire period. In detail, a Principal Component Analysis (PCA; Everitt and Hothorn, 2011; James et al., 2013) was performed on the annual means of the other FFR variables (air CO<sub>2</sub>, FCO2, RSAM) and the annual number of earthquakes to simplify and summarize the relationships among the multivariate set of data. We used the function *prcomp* of the package *stats* of the R software (R Core Team, 2021), which performs PCA via a singular value decomposition of the centered and scaled data matrix. This technique derives a new set of uncorrelated variables (Principal Components, PC) using a linear combination of the original variables, and ranks them in terms of their overall control on the variance. PCA is therefore used to reduce the dimensionality of the data set, by choosing only those PC that explain most of the variance in the data. In practice, the PCA applied to the 4-variables matrix returns 4 PC, which retain different proportions of the total variance: PC1 the 94.0%, PC2 the 3.6%, PC3 the 1.8%, and PC4 the 0.6% (Table 1). The scores of these new variables are calculated multiplying the matrix of the scaled original variables by the eigenvector matrix in Table 1 (namely, the eigenvectors of the correlation matrix of the original data set). These results indicate that nearly the total (temporal) variability of the data ( $\sim 94\%$ ) is explained by PC1 only, which is defined by an almost identical contribution of air CO<sub>2</sub>, RSAM, FCO2, and Earthquakes variables (see the coefficients of the first eigenvector in Table 1).

This suggests that a single driving mechanism controls the variations of hydrothermal fluid flux and earthquakes (Fig. 6), and as such summarizes well the temporal evolution of the hydrothermal part of the Cfc unrest. It is worth to note that PC1 is very well correlated with the Ptot and temperature, estimated using the *vapour-liquid coexistence* model (Fig. 6). We checked the reliability of this result by applying PCA to a larger number of observations, i.e., considering six months means of FFR variables and six months number of earthquakes, obtaining again a PC1 that explains a large portion of the variance (87%) and well correlating with Ptot and temperature. These results indicate that the correlation structure in the data is very

**Table 1**  
Principal Component Analysis (PCA). Results of the PCA applied to the variables FCO2, RSAM, air CO<sub>2</sub> and earthquakes.

Variables	Eigenvectors			
	PC1	PC2	PC3	PC4
FCO2	0.4993	0.3342	-0.7991	0.0215
RSAM	0.5100	-0.0659	0.2692	-0.8143
air CO <sub>2</sub>	0.4914	-0.7896	-0.0134	0.3672
earthquakes	0.4992	0.5103	0.5373	0.4491
Importance of components	PC1	PC2	PC3	PC4
Variance	3.7591	0.1430	0.0736	0.0243
Proportion of variance	0.9398	0.0357	0.0184	0.0061
Cumulative proportion	0.9398	0.9755	0.9939	1.0000

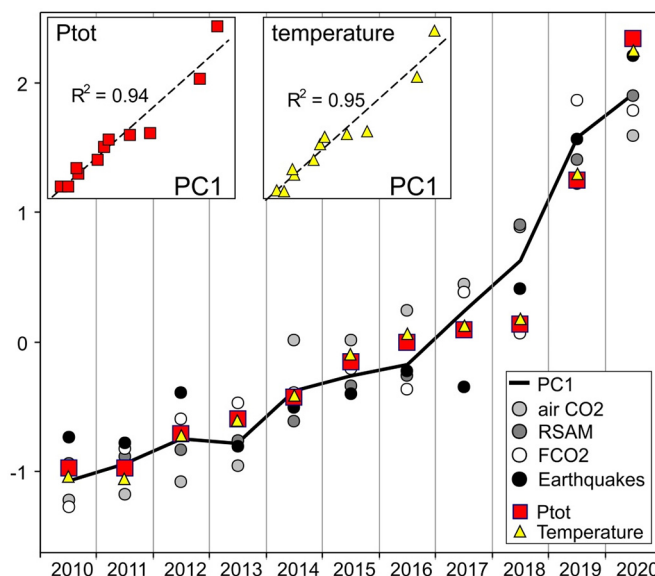


**Fig. 6.** Chronograms of the z-scores of the FFR variables (air CO<sub>2</sub>, RSAM, FCO2), earthquakes occurrence, PC1, and the Ptot-temperature estimations based on the *vapour-liquid coexistence* model (all the variables are reported as annual means; the z-score is equal to the variable minus the mean divided for the standard deviation). The FFR variables and the Earthquakes occurrence were analysed with a PCA and PC1 is the resulting main component explaining their 94% total variance. PC1 is plotted against Ptot and temperature in the insets.

strong and PCA, in the studied case, is stable also with a small number of observations.

Summarising, PCA results support our hypothesis that increasing fluid pressure and temperature in the hydrothermal system, due to an increasing input of magmatic gases, is a causal factor in triggering the Cfc seismicity, and is the driver for the observed escalation in hydrothermal fluid release at the surface.

In contrast, the *no-condensation* model outputs unrealistic results, as post-2015 estimated pressures are unacceptably low ( $<$  atmospheric pressure, 1 bar) and decrease over the same temporal interval during which earthquake occurrence rate and surface hydrothermal fluid fluxes are both visibly increasing. This mismatch indicates that the assumption that fumarolic water concentrations are currently fully representative of the deep, equilibrium compositions (Moretti et al., 2017) is inconsistent with the observations.

### 3.5. The conceptual model of the hydrothermal system and 'hydrothermal' seismicity

The conceptual model based on the *vapour-liquid coexistence* assumption is sketched in Fig. 7a over a 2-D resistivity model of Solfatara, derived by AMT (AudioMagnetotelluric) measurements (Siniscalchi et al., 2019). The section is dominated by a  $\sim 2$  km long vertically elongated resistivity structure in axis with Solfatara. This is the core of the hydrothermal system feeding the Solfatara-Pisciarelli hydrothermal sites. It is interpreted as a permeable zone that favours gas ascent from the hottest and deepest portions of the system. Hot, methane-free magmatic fluids enter the base ( $> 2$  km depth) of the system, mix with and vaporize meteoric liquids, and ultimately create the condition for CH<sub>4</sub> formation at temperatures  $> 360$  °C (Caliro et al., 2007). From that zone, a gas plume rises up to 0.3–0.7 km where the resistive structure is interrupted by conductive layers (green, cyan and blue colours) that reflect both hydrothermal altered zones and a liquid phase-dominated environment (Siniscalchi et al., 2019). It is worth noting that, assuming a hydrostatic control on fluid pressure, the inferred equilibration pressures of the *vapour-liquid coexistence* model (from 30 to 80 bar, considering both the DP and CV redox buffers, see section



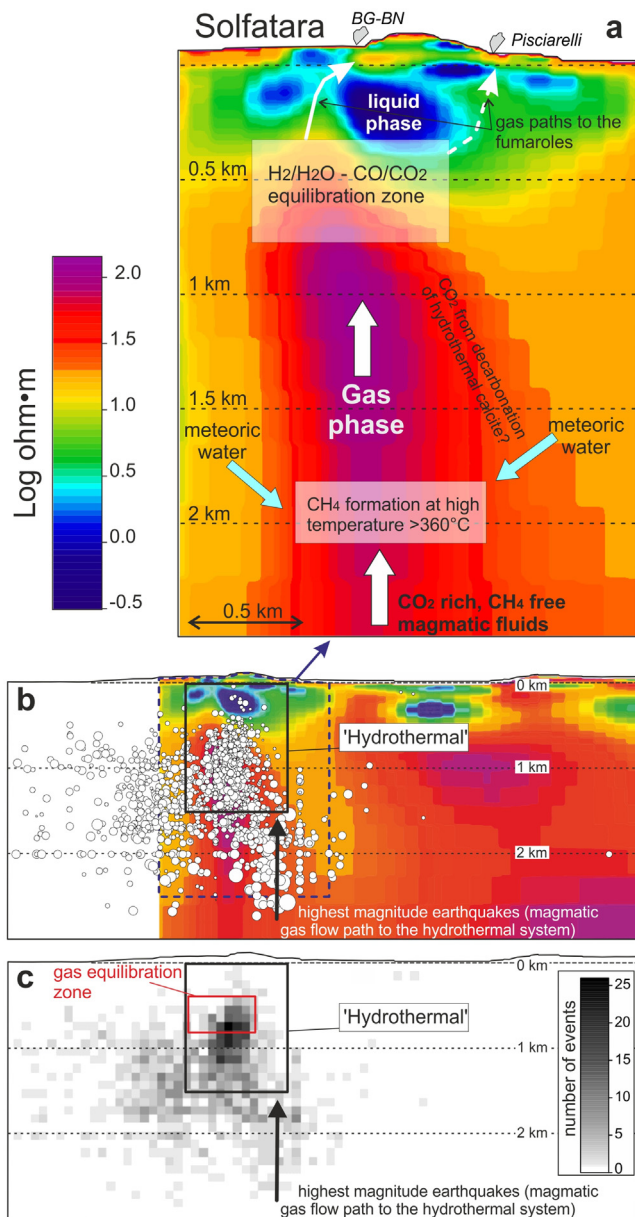


**Fig. 7.** Conceptual model and seismicity. a) Geochemical conceptual model of the hydrothermal system feeding the Solfatara-Pisciarelli manifestations sketched over a resistivity section (redrawn from Siniscalchi et al., 2019). b) section (A'-A" in Fig. 1A) showing the relations between earthquake location (distance <0.6 km from the section) and resistivity. The dimension of the white circles is proportional to the magnitude of the events. c) 2 D density map of earthquakes in the A'-A" section (computed as the number of events projected on cells of  $100 \times 100 \text{ m}^2$ ). The 'hydrothermal' box is a section of a parallelepiped of  $1.2 \times 1.2 \times 1.5 \text{ km}$  assumed to contain the hydrothermal system (see the text and Fig. 9).

3.1.2) correspond to gas equilibration depths of 0.3–0.8 km, that coincide with the top of the resistive structure (Fig. 7). Here, at the interface with the overlying clay-altered zones, the gas phase is expected to accumulate and to reside for a sufficient time to allow the gas phase to re-equilibrate at the local T-P conditions. From that zone, the gas moves toward the surface through fractures, shallow gas pockets and liquid bodies whose existence and complex geometry has been highlighted by detailed geo-electric surveys (Byrdina et al., 2014; Gresse et al., 2017, 2018).

According to (Chiodini et al., 2016), an escalating magmatic fluid inflow at the base of the hydrothermal system causes its heating and pressurization, and in turn the increase of the  $\text{CO}_2$  emission at the surface

and seismicity (Fig. 6). A dense earthquake cluster is observed at 0.5–1 km depth (Fig. 7b and c), and since this interval nicely corresponds to the gas equilibration depths inferred above (0.3–0.8 m) is here interpreted as the head of the gas front feeding the hydrothermal system. Thus, our inferred  $P_{\text{tot}}$  increase refers to such topmost portion of this seismogenic vertical gas plume. It is also noteworthy the existence of a second, deeper (>2 km) seismicity cluster that corresponds to the source area irradiating the highest magnitude earthquakes (Fig. 7b): this structure has been interpreted as the root of the gas plume, in which larger events are likely caused by pulsed magmatic fluid injections (e.g., Giudicepietro et al., 2020).

Ultimately, the close spatial correspondence between the main seismogenic volume (0.5–1 km) and the gas equilibration zone (0.3–0.8 km) supports the idea that, similarly to the seismicity induced by anthropogenic fluid injection, the generalised pressurization and heating of the CFc gas dominated-hydrothermal system act as the main seismicity trigger (Fig. 7b and c).

### 3.6. A mass balance of the steam associated with the $\text{CO}_2$ emission and hydrothermal seismicity

The observed escalation in surface gas release at Solfatara and Pisciarelli is an additional evident sign for increased gas transport at depth, and of a generalised gas pressure build-up at source. Using the numerous data of the  $\text{CO}_2$  emission from the target area (FCO2, Fig. 3a) we compute that the total  $\text{CO}_2$  emissions from Solfatara DDS increased from  $\sim 1000 \text{ t d}^{-1}$  in 2008–2010 up to  $3000\text{--}4000 \text{ t d}^{-1}$  in 2019–2020 (Fig. 8). Considering that similar increments also affected the fumarolic vents (Tamburello et al., 2019) we can roughly estimate the current total  $\text{CO}_2$  emission from Solfatara-Pisciarelli at  $\sim 5000 \text{ t d}^{-1}$ . This flux ranks CFc among the first 8 top volcanic  $\text{CO}_2$  emitters on Earth (Fischer et al., 2019; Werner et al., 2019). Such an unusually large gas supply implies pressure-build up in the gas source area (the hydrothermal system), and suggests an increased potential for phreatic explosions. Volatile supply must inherently be associated with a large thermal energy release (as steam and  $\text{CO}_2$  are associated prior to condensation). We stress that since gas pressurization is an exothermic process, it may itself be causing heating. In addition, the pressurization of a steam-rich gas phase can induce its condensation, a process that at CFc hydrothermal system is described by the vapour-liquid coexistence geochemical model. Condensation can be shallow (forming the hot soils and mud pools that characterise the fumarolic fields) or relatively

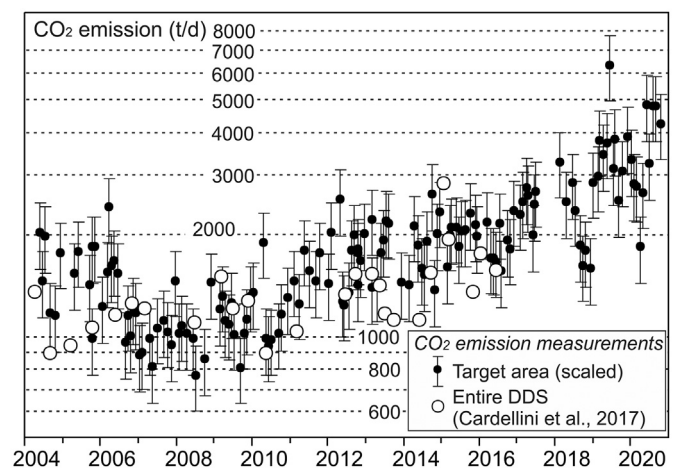


**Fig. 8.**  $\text{CO}_2$  emission from diffuse degassing at Solfatara DDS during 2004–2020. The black dots refer to the emission from the target area (Fig. 1 and Fig. 3a) scaled over the entire DDS. This was possible by elaborating the data of the 30 campaigns reported in (Cardellini et al., 2017). From these data we computed the mean ratio between the DDS emission and that from the target area ( $4.7 \pm 1.1$ ), that is used as correction factor (error bars refer to the standard deviation of the correction factor).

deep. We attempt at establishing a steam mass balance for the hydrothermal systems by dividing it into 3 components (Fig. 9a):

- the original steam emission at reservoir conditions (*reservoir emission* in Fig. 9a); this is derived by multiplying the diffuse CO<sub>2</sub> flux (FCO<sub>2</sub>-DDS) by the H<sub>2</sub>O/CO<sub>2</sub> ratio in the gas equilibration zone (derived from P<sub>H<sub>2</sub>O</sub> and P<sub>CO<sub>2</sub></sub> estimates);
- the fraction of steam condensing in the sub-surface of the DDS (*DDS condensate* in Fig. 9a); this computed by multiplying FCO<sub>2</sub>-DDS by the fumarolic H<sub>2</sub>O/CO<sub>2</sub>;
- the fraction of steam that condense at depth (*deep condensate* in Fig. 9a, b and c); given by the difference *reservoir emission* - *DDS condensate*.

It is worth to note that the inferred temporal evolution of the *deep condensate* mass matches nicely that of 'hydrothermal' seismicity (Fig. 9b and c), i.e., of the events occurred in the volume containing the hydrothermal system (see Fig. 7b and c). In our interpretation, the *deep condensate* represents the fraction of the original steam/thermal energy budget that can potentially trigger earthquakes because the condensed liquid can lubricate pre-existing fractures and because hydrothermal host rocks get hotter, increase in volume by

thermal dilatation, and finally fracture as they reach a failure threshold. The total thermal energy involved in *deep condensate* from 2004 to 2020 is  $\sim 4 \times 10^{14}$  J (computed from the latent heat of condensation), and is thus well enough to justify the observed seismicity (being 5 orders of magnitude higher than the cumulative energy of all the CFC earthquakes,  $\sim 1.5 \times 10^9$  J, [http://www.ov.ingv.it/ov/bollettini-mensili-campania/Bollettino\\_Mensile\\_Campi\\_Flegrei\\_2020\\_10.pdf](http://www.ov.ingv.it/ov/bollettini-mensili-campania/Bollettino_Mensile_Campi_Flegrei_2020_10.pdf)).

#### 4. Conclusions

We use a novel multidisciplinary approach to characterise the spatial-temporal evolution of the hydrothermal unrest currently affecting CFC. Use of such a multidisciplinary methodology at CFC is facilitated by the especially robust and continuous records available for both geochemical parameters (including fumarolic compositions, soil CO<sub>2</sub> fluxes and fluid flow related variables), and seismicity. Although these multiple dataset may not all simultaneously be available at many of the degassing restless calderas worldwide, we yet conclude our approach is general, and may find application provided at least fumarolic gas compositions, soil flux emissions and seismic catalogues are available.

In the CFC example, a multivariate analysis shows that the different datasets share a common evolution during 2010–2020, and are fully described by a single component that explains 94% of their total variance. This component, whose values exhibit a sharp increase from 2018 onward, is well correlated with escalating pressure and temperature of the hydrothermal system inferred from geochemical modelling of fumarole composition. The P-T increase occurs in a gas-dominated zone, located at depths of <1 km below the main hydrothermal sites, which corresponds to the main cluster of low magnitude, post 2004 earthquakes. This temporal and spatial association between hydrothermal P-T and seismicity brings compelling evidence for the role played by pressurising hydrothermal fluids in driving volcano seismicity at CFC. Our results bring evidence for the seismogenetic role played by magmatic gas injection into hydrothermal systems, and are thus of general relevance for other volcanoes in similar contexts.

#### Authors contribution

G.C. originally conceived the study and wrote the manuscript with the help of A.A., C.C., G.B., J.S., Z.P., F.G.;  
F.G. and W.D.C. analysed RSAM;  
R.A., S.C. and G.C. sampled and analysed the fumaroles and interpreted the compositions;  
R.A. and C.C. measured gas diffuse emissions;  
P.R. analysed the earthquakes;  
G.B. and J.S. performed PCA;  
A.S., S.T. and Z.P. measured and interpreted the AMT data;  
All the authors contributed to the discussion.

#### Funding

This work was supported by MIUR, project n. PRIN2017-2017LMNLAW "Connect4Carbon". Most of the used data were acquired in the frame of the Campi Flegrei volcanic surveillance funded by the Italian Dipartimento della Protezione Civile, Presidenza del Consiglio dei Ministri (DPC). This paper does not necessarily represent DPC official opinion and policies.

#### Declaration of Competing Interest

The authors declare that they have no known competing financial interests or personal relationships that could have appeared to influence the work reported in this paper.

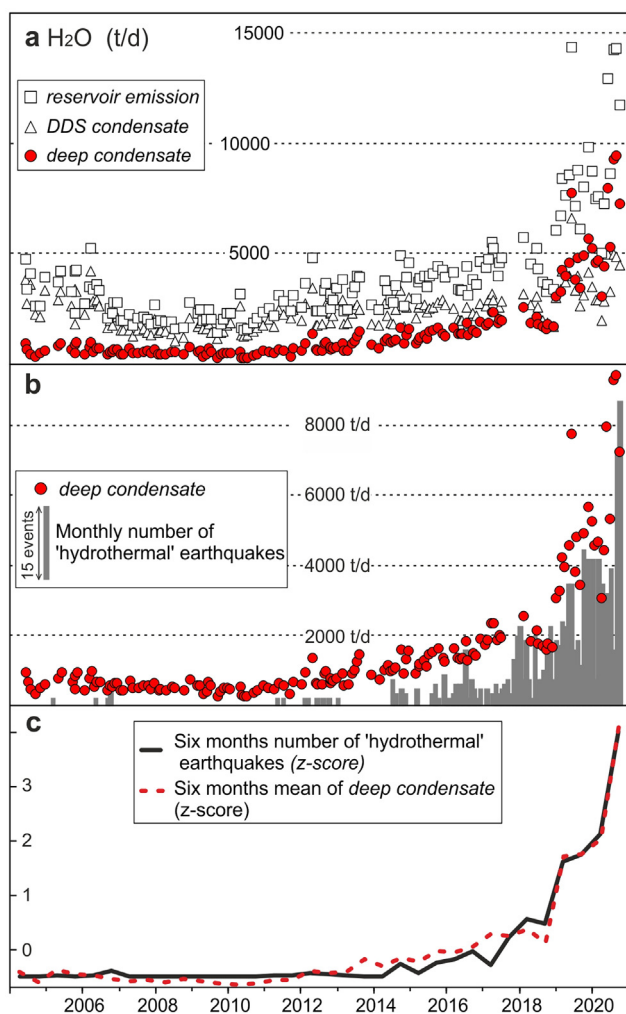


**Fig. 9.** Deep condensation rate and hydrothermal earthquakes occurrence. a) results of the steam mass balance involved in the degassing process (see the text). b) *Deep condensate* rate vs the monthly number of 'hydrothermal' earthquakes (gray histogram). c) Normalized 'hydrothermal' earthquakes occurrence and normalized mean of *deep condensate* rate (six month values). See Fig. 7 for the definition of 'hydrothermal' earthquakes.



## Acknowledgments

We would like to remember the researchers Roberto Cioni and Egizio Corazza who recently passed away: they began to sample and analyze Solfatara fumaroles in early 1980's, starting the Solfatara fumaroles database. We thank Bruce Christenson and an anonymous reviewer for their insightful comments. This work is part of the INGV research project LOVE-CF (Linking surface Observables to sub-Volcanic plumbing-system: a multidisciplinary approach for Eruption forecasting at Campi Flegrei caldera (Italy)).

## Appendix A. Supplementary data

Supplementary data to this article can be found online at <https://doi.org/10.1016/j.jvolgeores.2021.107245>.

## References

- Aiuppa, A., Tamburello, G., Di Napoli, R., Cardellini, C., Chiodini, G., Giudice, G., Grassa, F., Pedone, M., 2013. First observations of the fumarolic gas output from a restless caldera: Implications for the current period of unrest (2005–2013) at Campi Flegrei. *Geochem. Geophys. Geosyst.* 14 (10), 4153–4169. <https://doi.org/10.1002/ggge.20261>.
- Aiuppa, A., Fiorani, L., Santoro, S., Parracino, S., Nuvoli, M., Chiodini, G., Minopoli, C., Tamburello, G., 2015. New ground-based lidar enables volcanic CO<sub>2</sub> flux measurements. *Sci. Rep.* 5. <https://doi.org/10.1038/srep13614>.
- Amoruso, A., Crescentini, L., Sabbetta, I., 2014a. Paired deformation sources of the Campi Flegrei caldera (Italy) required by recent (1980–2010) deformation history. *J. Geophys. Res.* 119 (2), 858–879. <https://doi.org/10.1002/2013JB010392>.
- Amoruso, A., Crescentini, L., Sabbetta, I., De Martino, P., Obrizzo, F., Tammaro, U., 2014b. Clues to the cause of the 2011–2013 Campi Flegrei caldera unrest, Italy, from continuous GPS data. *Geophys. Res. Lett.* 41, 3081–3088. <https://doi.org/10.1002/2014GL059539>.
- Bianco, F., Del Pezzo, E., Saccorotti, G., Ventura, G., 2004. The role of hydrothermal fluids in triggering the July–August 2000 seismic swarm at Campi Flegrei, Italy: evidence from seismological and mesostructural data. *J. Volcanol. Geotherm. Res.* 133 (1), 229–246. [https://doi.org/10.1016/S0377-0273\(03\)00400-1](https://doi.org/10.1016/S0377-0273(03)00400-1).
- Bruno, P.P.G., Ricciardi, G.P., Petrillo, Z., Di Fiore, V., Troiano, A., Chiodini, G., 2007. Geophysical and hydrogeological experiments from a shallow hydrothermal system at Solfatara Volcano, Campi Flegrei, Italy: Response to caldera unrest. *J. Geophys. Res.* 112 (B6). <https://doi.org/10.1029/2006JB004383>.
- Byrdina, S., Vandemeulebrouck, J., Cardellini, C., Legaz, A., Camerlynck, C., Chiodini, G., Lebourg, T., Gresse, M., Bascou, P., Motos, G., Carrier, A., Caliro, S., 2014. Relations between electrical resistivity, carbon dioxide flux, and self-potential in the shallow hydrothermal system of Solfatara (Phlegrean Fields, Italy). *J. Volcanol. Geotherm. Res.* 283, 172–182. <https://doi.org/10.1016/j.jvolgeores.2014.07.010>.
- Caliro, S., Chiodini, G., Moretti, R., Avino, R., Granieri, D., Russo, M., Fiebig, J., 2007. The origin of the fumaroles of La Solfatara (Campi Flegrei, South Italy). *Geochim. Cosmochim. Acta* 71 (12), 3040–3055. <https://doi.org/10.1016/j.gca.2007.04.007>.
- Caliro, S., Chiodini, G., Paonita, A., 2014. Geochemical evidences of magma dynamics at Campi Flegrei (Italy). *Geochim. Cosmochim. Acta* 132, 1–15. <https://doi.org/10.1016/j.gca.2014.01.021>.
- Cardellini, C., Chiodini, G., Frondini, F., 2003. Application of stochastic simulation to CO<sub>2</sub> flux from soil: Mapping and quantification of gas release. *J. Geophys. Res.* 108 (B9). <https://doi.org/10.1029/2002JB002165>.
- Cardellini, C., Chiodini, G., Frondini, F., Avino, R., Bagnato, E., Caliro, S., Lelli, M., Rosiello, A., 2017. Monitoring diffuse volcanic degassing during volcanic unrests: the case of Campi Flegrei (Italy). *Sci. Rep.* 7 (1). <https://doi.org/10.1038/s41598-017-06941-2>.
- Castaldo, R., D'Auria, L., Pepe, S., Solaro, G., De Novellis, V., Tizzani, P., 2019. The impact of crustal rheology on natural seismicity: Campi Flegrei caldera case study. *Geosci. Front.* 10 (2), 453–466. <https://doi.org/10.1016/j.gsf.2018.02.003>.
- Chiodini, G., Marini, L., 1998. Hydrothermal gas equilibria: the H<sub>2</sub>O–H<sub>2</sub>–CO<sub>2</sub>–CO–CH<sub>4</sub> system. *Geochim. Cosmochim. Acta* 62 (15), 2673–2687. [https://doi.org/10.1016/S0016-7037\(98\)00181-1](https://doi.org/10.1016/S0016-7037(98)00181-1).
- Chiodini, G., Cioni, R., Magro, G., Marini, L., Panichi, C., Raco, B., Russo, M., 1996. Chemical and isotopic variations of Bocca Grande fumarole (Solfatara Volcano, Phlegrean Fields). *Acta Vulcanol.* 8, 129–138.
- Chiodini, G., Cioni, R., Guidi, M., Raco, B., Marini, L., 1998. Soil CO<sub>2</sub> flux measurements in volcanic and geothermal areas. *Appl. Geochem.* 13 (5), 543–552. [https://doi.org/10.1016/S0883-2927\(97\)00076-0](https://doi.org/10.1016/S0883-2927(97)00076-0).
- Chiodini, G., Frondini, F., Cardellini, C., Granieri, D., Marini, L., Ventura, G., 2001. CO<sub>2</sub> degassing and energy release at Solfatara volcano, Campi Flegrei, Italy. *J. Geophys. Res.* 106 (B8), 16213–16221. <https://doi.org/10.1029/2001JB000246>.
- Chiodini, G., Vandemeulebrouck, J., Caliro, S., D'Auria, L., De Martino, P., Mangiacapra, A., Petrillo, Z., 2015. Evidence of thermal-driven processes triggering the 2005–2014 unrest at Campi Flegrei caldera. *Earth Planet. Sci. Lett.* 414, 58–67. <https://doi.org/10.1016/j.epsl.2015.01.012>.
- Chiodini, G., Paonita, A., Aiuppa, A., Costa, A., Caliro, S., De Martino, P., Acocella, V., Vandemeulebrouck, J., 2016. Magmas near the critical degassing pressure drive volcanic unrest towards a critical state. *Nat. Commun.* 7. <https://doi.org/10.1038/ncomms13712>.
- Chiodini, G., Selva, J., Del Pezzo, E., Marsan, D., De Siena, L., D'Auria, L., Bianco, F., Caliro, S., De Martino, P., Ricciolino, P., Petrillo, Z., 2017a. Clues on the origin of post-2000 earthquakes at Campi Flegrei caldera (Italy). *Sci. Rep.* 7 (1). <https://doi.org/10.1038/s41598-017-04845-9>.
- Chiodini, G., Giudicepietro, F., Vandemeulebrouck, J., Aiuppa, A., Caliro, S., De Cesare, W., Tamburello, G., Avino, R., Orazi, M., D'Auria, L., 2017b. Fumarolic tremor and geochemical signals during a volcanic unrest. *Geology* 45 (12), 1131–1134. <https://doi.org/10.1130/G39447.1>.
- Chiodini, G., Cardellini, C., Di Luccio, F., Selva, J., Frondini, F., Caliro, S., Rosiello, A., Beddini, G., Ventura, G., 2020. Correlation between tectonic CO<sub>2</sub> Earth degassing and seismicity is revealed by a 10-year record in the Apennines, Italy. *Sci. Adv.* 6 (35). <https://doi.org/10.1126/sciadv.abc2938> eabc2938.
- Cioni, R., Corazza, E., 1981. Medium-temperature fumarolic gas sampling. *Bull. Volcanol.* 44 (1), 23–29. <https://doi.org/10.1007/BF02598186>.
- Cioni, R., Corazza, E., Marini, L., 1984. The gas/steam ratio as indicator of heat transfer at the Solfatara fumaroles, Phlegrean Fields (Italy). *Bull. Volcanol.* 47, 295–302. <https://doi.org/10.1007/BF01961560>.
- Costa, A., Folch, A., Macedonio, G., Giaccio, B., Isaia, R., Smith, V.C., 2012. Quantifying volcanic ash dispersal and impact of the Campanian Ignimbrite super-eruption. *Geophys. Res. Lett.* 39 (10). <https://doi.org/10.1029/2012GL051605>.
- D'Amore, F., Panichi, C., 1980. Evaluation of deep temperatures of hydrothermal systems by a new gas geothermometer. *Geochim. Cosmochim. Acta* 44 (3), 549–556. [https://doi.org/10.1016/0016-7037\(80\)90051-4](https://doi.org/10.1016/0016-7037(80)90051-4).
- D'Auria, L., Giudicepietro, F., Aquino, I., Borriello, G., Del Gaudio, C., Lo Bascio, D., Martini, M., Ricciardi, G.P., Ricciolino, P., Ricco, C., 2011. Repeated fluid-transfer episodes as a mechanism for the recent dynamics of Campi Flegrei caldera (1989–2010). *J. Geophys. Res.* 116 (B4). <https://doi.org/10.1029/2010JB007837>.
- Del Gaudio, C., Aquino, I., Ricciardi, G.P., Ricco, C., Scandone, R., 2010. Unrest episodes at Campi Flegrei: a reconstruction of vertical ground movements during 1905–2009. *J. Volcanol. Geotherm. Res.* 195 (1), 48–56. <https://doi.org/10.1016/j.jvolgeores.2010.05.014>.
- Deutsch, C.V., Journel, A.G., 1998. *GSLIB: Geostatistical Software Library and Users Guide*. Oxford University Press, Oxford, New York 369 pp.
- Ellsworth, W.L., 2013. Injection-Induced Earthquakes. *Science* 341 (6142), 1225942. <https://doi.org/10.1126/science.1225942>.
- Endo, E.T., Murray, T., 1991. Real-time Seismic Amplitude Measurement (RSAM): a volcano monitoring and prediction tool. *Bull. Volcanol.* 53 (7), 533–545. <https://doi.org/10.1007/BF00298154>.
- Everitt, B., Hothorn, T., 2011. *An Introduction to Applied Multivariate Analysis with R*. Springer, New York 274 pp.
- Farrar, C.D., Sorey, M.L., Evans, W.C., Howle, J.F., Kerr, B.D., Kennedy, B.M., King, C.Y., Southon, J.R., 1995. Forest-killing diffuse CO<sub>2</sub> emission at Mammoth Mountain as a sign of magmatic unrest. *Nature* 376 (6542), 675–678. <https://doi.org/10.1038/376675a0>.
- Fischer, T., Matyska, C., Heinicke, J., 2017. Earthquake-enhanced permeability – evidence from carbon dioxide release following the M<sub>L</sub> 3.5 earthquake in West Bohemia. *Earth Planet. Sci. Lett.* 460, 60–67. <https://doi.org/10.1016/j.epsl.2016.12.001>.
- Fischer, T.P., Arellano, S., Carn, S., Aiuppa, A., Galle, B., Allard, P., Lopez, T., Shinohara, H., Kelly, P., Werner, C., Cardellini, C., Chiodini, G., 2019. The emissions of CO<sub>2</sub> and other volatiles from the world's subaerial volcanoes. *Sci. Rep.* 9 (1), 18716. <https://doi.org/10.1038/s41598-019-54682-1>.
- Giggenbach, W.F., 1980. Geothermal gas equilibria. *Geochim. Cosmochim. Acta* 44, 2021–2032. [https://doi.org/10.1016/0016-7037\(80\)90200-8](https://doi.org/10.1016/0016-7037(80)90200-8).
- Giggenbach, W.F., 1987. Redox processes governing the chemistry of fumarolic gas discharges from White Island, New Zealand. *Appl. Geochem.* 2 (2), 143–161. [https://doi.org/10.1016/0883-2927\(87\)90030-8](https://doi.org/10.1016/0883-2927(87)90030-8).
- Girault, F., Adhikari, L.B., France-Lanord, C., Agrinier, P., Koirala, B.P., Bhattarai, M., Mahat, S.S., Groppo, C., Rolfo, F., Bollinger, L., Perrier, F., 2018. Persistent CO<sub>2</sub> emissions and hydrothermal unrest following the 2015 earthquake in Nepal. *Nat. Commun.* 9 (1), 2956. <https://doi.org/10.1038/s41467-018-05138-z>.
- Giudicepietro, F., Chiodini, G., Caliro, S., De Cesare, W., Esposito, A.M., Galluzzo, D., Lo Bascio, D., Macedonio, G., Orazi, M., Ricciolino, P., Vandemeulebrouck, J., 2019. Insight into Campi Flegrei caldera unrest through seismic tremor measurements at pisciarelli fumarolic field. *Geochim. Geophys. Geosyst.* 20 (11), 5544–5555. <https://doi.org/10.1029/2019GC008610>.
- Giudicepietro, F., Chiodini, G., Avino, R., Brandi, G., Caliro, S., De Cesare, W., Galluzzo, D., Esposito, A., La Rocca, A., Lo Bascio, D., Obrizzo, F., Pinto, P., Ricci, T., Ricciolino, P., Siniscalchi, A., Tramelli, A., Vandemeulebrouck, J., Macedonio, G., 2020. Tracking episodes of seismicity and gas transport in Campi Flegrei caldera through seismic, geophysical and geochemical measurements. *Seismol. Res. Lett.*, 1–11. <https://doi.org/10.1785/0220200223> in press.
- Granieri, D., Avino, R., Chiodini, G., 2009. Carbon dioxide diffuse emission from the soil: ten years of observations at Vesuvio and Campi Flegrei (Pozzuoli), and linkages with volcanic activity. *Bull. Volcanol.* 72 (1), 103. <https://doi.org/10.1007/s00445-009-0304-8>.
- Gresse, M., Vandemeulebrouck, J., Byrdina, S., Chiodini, G., Revil, A., Johnson, T.C., Ricci, T., Vilardo, G., Mangiacapra, A., Lebourg, T., Grangeon, J., Bascou, P., Metral, L., 2017. Three-Dimensional Electrical Resistivity Tomography of the Solfatara Crater (Italy): Implication for the Multiphase Flow Structure of the Shallow Hydrothermal System. *J. Geophys. Res.* 122 (11), 8749–8768. <https://doi.org/10.1002/2017JB014389>.
- Gresse, M., Vandemeulebrouck, J., Byrdina, S., Chiodini, G., Roux, P., Rinaldi, A.P., Wathelet, M., Ricci, T., Letort, J., Petrillo, Z., Tuccimei, P., Lucchetti, C., Sciarra, A., 2018. Anatomy of a fumarolic system inferred from a multiphysics approach. *Sci. Rep.* 8 (1), 7580. <https://doi.org/10.1038/s41598-018-25448-y>.

- Hotovec-Ellis, A.J., Shelly, D.R., Hill, D.P., Pitt, A.M., Dawson, P.B., Chouet, B.A., 2018. Deep fluid pathways beneath Mammoth Mountain, California, illuminated by migrating earthquake swarms. *Sci. Adv.* 4 (8). <https://doi.org/10.1126/sciadv.aat5258> eaat5258.
- Hubbert, M., Rubey, W., 1959. Role of fluid pressure in mechanics of overthrust faulting. *Geol. Soc. Am.* 70, 115–166.
- James, G., Witten, D., Hastie, T., Tibshirani, R., 2013. *An Introduction to Statistical Learning*. Springer, New York 426 pp.
- Keranen, K.M., Weingarten, M., 2018. Induced Seismicity. *Annu. Rev. Earth Planet. Sci.* 46 (1), 149–174. <https://doi.org/10.1146/annurev-earth-082517-010054>.
- Kilburn, C.R.J., De Natale, G., Carlino, S., 2017. Progressive approach to eruption at Campi Flegrei caldera in southern Italy. *Nat. Commun.* 8 (1), 15312. <https://doi.org/10.1038/ncomms15312>.
- Lewicki, J.L., Hilley, G.E., Shelly, D.R., King, J.C., McGeehin, J.P., Mangan, M., Evans, W.C., 2014. Crustal migration of CO<sub>2</sub>-rich magmatic fluids recorded by tree-ring radiocarbon and seismicity at Mammoth Mountain, CA, USA. *Earth Planet. Sci. Lett.* 390, 52–58. <https://doi.org/10.1016/j.epsl.2013.12.035>.
- Miller, S.A., 2013. The role of fluids in tectonic and earthquake processes. In: Dmowska, R. (Ed.), *Advanc. Geophys. Advances in Geophysics*, pp. 1–46 <https://doi.org/10.1016/b978-0-12-380940-7.00001-9>.
- Moretti, R., De Natale, G., Troise, C., 2017. A geochemical and geophysical reappraisal to the significance of the recent unrest at Campi Flegrei caldera (Southern Italy). *Geochem. Geophys. Geosyst.* 18 (3), 1244–1269. <https://doi.org/10.1002/2016GC006569>.
- Orsi, G., Civetta, L., Del Gaudio, C., de Vita, S., Di Vito, M.A., Isaia, R., Petrazzuoli, S.M., Ricciardi, G.P., Ricco, C., 1999. Short-term ground deformations and seismicity in the resurgent Campi Flegrei caldera (Italy): an example of active block-resurgence in a densely populated area. *J. Volcanol. Geotherm. Res.* 91 (2), 415–451. [https://doi.org/10.1016/S0377-0273\(99\)00050-5](https://doi.org/10.1016/S0377-0273(99)00050-5).
- Pedone, M., Aiuppa, A., Giudice, G., Grassa, F., Cardellini, C., Chiodini, G., Valenza, M., 2014. Volcanic CO<sub>2</sub> flux measurement at Campi Flegrei by tunable diode laser absorption spectroscopy. *Bull. Volcanol.* 76 (4). <https://doi.org/10.1007/s00445-014-0812-z>.
- Pfeiffer, L., Wanner, C., Lewicki, J.L., 2018. Unraveling the dynamics of magmatic CO<sub>2</sub> degassing at Mammoth Mountain, California. *Earth Planet. Sci. Lett.* 484, 318–328. <https://doi.org/10.1016/j.epsl.2017.12.038>.
- QueiSer, M., Granieri, D., Burton, M., Arzilli, F., Avino, R., Carandente, A., 2017. Increasing CO<sub>2</sub> flux at Pisciarelli, Campi Flegrei, Italy. *Solid Earth* 8 (5), 1017–1024. <https://doi.org/10.5194/se-8-1017-2017>.
- R Core Team, 2021. *R: A Language and Environment for Statistical Computing*. R Foundation for Statistical Computing, Vienna, Austria.
- Saccorotti, G., Petrosino, S., Bianco, F., Castellano, M., Galluzzo, D., La Rocca, M., Del Pezzo, E., Zaccarelli, L., Cusano, P., 2007. Seismicity associated with the 2004–2006 renewed ground uplift at Campi Flegrei Caldera. Italy. *Phys. Earth Planet. Inter.* 165 (1), 14–24. <https://doi.org/10.1016/j.pepi.2007.07.006>.
- Selva, J., Marzocchi, W., Papale, P., Sandri, L., 2012. Operational eruption forecasting at high-risk volcanoes: the case of Campi Flegrei. Naples. *J. App. Volcanol.* 1 (1), 5. <https://doi.org/10.1186/2191-5040-1-5>.
- Sibson, R.H., 1992. Implications of fault-valve behaviour for rupture nucleation and recurrence. *Tectonophysics* 211, 283–293. [https://doi.org/10.1016/0040-1951\(92\)90065-E](https://doi.org/10.1016/0040-1951(92)90065-E).
- Siniscalchi, A., Tripaldi, S., Romano, G., Chiodini, G., Improta, L., Petrillo, Z., D'Auria, L., Caliro, S., Avino, R., 2019. Reservoir Structure and Hydraulic Properties of the Campi Flegrei Geothermal System Inferred by Audiomagnetotelluric, Geochemical, and Seismicity Study. *J. Geophys. Res.* 124 (6), 5336–5356. <https://doi.org/10.1029/2018JB016514>.
- Smith, V.C., Isaia, R., Pearce, N.J.G., 2011. Tephrostratigraphy and glass compositions of post-15 kyr Campi Flegrei eruptions: implications for eruption history and chronostratigraphic markers. *Quat. Sci. Rev.* 30 (25), 3638–3660. <https://doi.org/10.1016/j.quascirev.2011.07.012>.
- Sorey, M.L., Evans, W.C., Kennedy, B.M., Farrar, C.D., Hainsworth, L.J., Hausback, B., 1998. Carbon dioxide and helium emissions from a reservoir of magmatic gas beneath Mammoth Mountain, California. *J. Geophys. Res.* 103 (7), 15303–15323. <https://doi.org/10.1029/98JB01389>.
- Stull, D.R., Westrum, E.F., Sinke, G.G., 1969. *The Chemical Thermodynamics of Organic Compounds*. Wiley, New York 865 pp.
- Tamburello, G., Caliro, S., Chiodini, G., De Martino, P., Avino, R., Minopoli, C., Carandente, A., Rouwet, D., Aiuppa, A., Costa, A., Bitetto, M., Giudice, G., Francofonte, V., Ricci, T., Sciarra, A., Bagnato, E., Capecchiacci, F., 2019. Escalating CO<sub>2</sub> degassing at the Pisciarelli fumarolic system, and implications for the ongoing Campi Flegrei unrest. *J. Volcanol. Geotherm. Res.* 384, 151–157. <https://doi.org/10.1016/j.jvolgeores.2019.07.005>.
- Werner, C., Bergfeld, D., Farrar, C.D., Doukas, M.P., Kelly, P.J., Kern, C., 2014. Decadal-scale variability of diffuse CO<sub>2</sub> emissions and seismicity revealed from long-term monitoring (1995–2013) at Mammoth Mountain, California, USA. *J. Volcanol. Geotherm. Res.* 289, 51–63. <https://doi.org/10.1016/j.jvolgeores.2014.10.020>.
- Werner, C., Fischer, T.P., Aiuppa, A., Edmonds, M., Cardellini, C., Carn, S., Chiodini, G., Cottrell, E., Burton, M., Shinohara, H., Allard, P., 2019. Carbon dioxide emissions from subaerial volcanic regions: two decades in review. In: Orcutt, B.N., Daniel, I., Dasgupta, R. (Eds.), *Deep Carbon: Past to Present*. Cambridge University Press, Cambridge, pp. 188–236 <https://doi.org/10.1017/9781108677950>.